Geofísica Internacional (2026) **65-2**: 2113- 2129

Ground Subsidence and Earthquake Induced Settlements in Mexico City, Using Satellite Imagery

Alberto Jaime-Paredes, Gaspar Alcocer-Gómez and Juan S. Sanabria-Pérez

Abstract

This study presents an integrated analysis of ground subsidence and earthquake-induced settlements in Mexico City using Differential Interferometric Synthetic Aperture Radar (DInSAR) techniques applied to Sentinel-1 satellite imagery. Subsidence in the Valley of Mexico-primarily caused by groundwater overexploitation-has historically led to significant structural damage across the urban landscape. While conventional monitoring methods such as benchmark leveling are effective, they are time- and resource-intensive. In this work, open-access Sentinel-1 data and the SNAP toolbox developed by the European Space Agency (ESA) were used to assess regional subsidence throughout 2016 and to identify sudden displacements linked to the September 2017 seismic events. Satellite-derived measurements were validated against historical benchmark data. The results demonstrate that DInSAR reliably captures both gradual subsidence patterns and abrupt, earthquake-related settlements, notably in the Historic Center and the vicinity of the Xico Volcano. Annual subsidence rates reached up to 0.45 m in some areas, while earthquake-induced deformations ranged from 0.01 to a 0.05 m. These findings highlight the effectiveness of satellite-based remote sensing as a cost-efficient and robust tool for ground subsidence monitoring in urban environments.

Key words: ground subsidence, earthquakes, seismic-induced settlement, line of sight, benchmarks, SAR imagery, DInSAR.

Resumen

Este estudio presenta un análisis integrado del hundimiento del terreno y los asentamientos provocados por sismos en la Ciudad de México utilizando técnicas de radar interferométrico sintético diferencial (DInSAR) aplicadas a imágenes satelitales del Sentinel-1. La subsidencia en el valle de México, causada principalmente por la sobreexplotación de las aguas subterráneas, ha provocado históricamente importantes daños estructurales en todo el paisaje urbano. Si bien los métodos de monitoreo convencionales, como la nivelación de puntos de referencia, son eficaces, requieren mucho tiempo y recursos. En este trabajo, se utilizaron datos de acceso abierto de Sentinel-1 y el programa SNAP desarrollado por la Agencia Espacial Europea (ESA) para evaluar la subsidencia regional a lo largo de 2016 e identificar desplazamientos repentinos relacionados con los eventos sísmicos de septiembre de 2017. Las mediciones obtenidas por satélite se validaron con datos históricos de referencia. Los resultados demuestran que DInSAR captura de forma confiable tanto los patrones de subsidencia gradual como los súbitos relacionados con los sismos, especialmente en el centro histórico y en las proximidades del volcán Xico. Las tasas de subsidencia anuales alcanzaron hasta 0.45 m en algunas zonas, mientras que las deformaciones inducidas por los sismos oscilaron entre 0.01 y 0.05 m. Estos hallazgos resaltan la eficacia del monitoreo remoto por satélite como herramienta rentable y sólida para la vigilancia de la subsidencia en entornos urbanos.

Palabras clave: Subsidencia, sismos, asentamientos inducidos por sismos, línea de visión, puntos de referencia, imagenes SAR, DInSAR.

Received: August 28, 2024; Accepted: December 28, 2025; Published on-line: April 1, 2026.

Editorial responsibility: Dr. Enrique Cabral Cano

* Corresponding author: Juan S. Sanabria-Pérez, juan.sanabria@comunidad.unam.mx
[1] Colegio de Ingenieros Civiles de México, Ciudad de México, México.
[2] Universidad Autónoma de Yucatán, Mérida-Yucatán, México.
[3] Universidad Nacional Autónoma de México, Posgrado de Ingeniería, Ciudad de México, México.

Alberto Jaime-Paredes, Gaspar Alcocer-Gómez, Juan Sandino Sanabria Pérez

https://doi.org/10.22201/igeof.2954436xe.2026.65.2.1819

1. Introduction

1.1 Background

Subsidence in Mexico City has caused significant damage to buildings, water supply and drainage systems, public transportation, streets, and other infrastructure. Measuring subsidence rates across different areas of the city is essential for assessing how these structures are affected. Traditionally, monitoring has been carried out using conventional topographic methods. Institutions such as the extinct Secretariat of Hydraulic Resources, the National Water Commission, the Water Management Office of the Valley of Mexico (now the Basin Organization of Water of the Valley of Mexico), and the Water System of Mexico City (SACMEX) have conducted topographic leveling over various periods up to the present. However, these methods are costly and time-consuming. Satellite imagery provides a faster and more cost-effective alternative for monitoring subsidence.

Additionally, the Valley of Mexico is located in a region of high seismicity. Significant earthquakes that have caused damage in Mexico City were recorded in 1957, 1985, and more recently in 2017 (Quintanar *et al.*, 2024). These events resulted in damage to buildings, potable water pipelines, streets, and other municipal infrastructure systems.

1.2 Objective

To demonstrate that it is possible to obtain useful and technically satisfactory results for land subsidence monitoring as well as settlement caused by earthquakes using the DInSAR technique, employing free satellite imagery and open-access software. This approach enables efficient topographic and geotechnical monitoring at very low cost and within short timeframes, which is particularly relevant for institutions, municipalities, and regional authorities. Accordingly, the article aims to highlight the operational viability of this technology as a supporting tool in urban risk management.

1.3 Scope

This article addresses the subsidence in Mexico City caused by the overexploitation of aquifers to supply potable water to the city. Using the DInSAR technique, subsidence rates in various areas of the city are determined and compared with those obtained through conventional topography via benchmark leveling, measurements, and published information on the settlements in Mexico City. The basic principles and methodology of satellite image processing are presented. Additionally, the sudden subsidence caused by the earthquakes of September 2017 is determined.

2. Regional Subsidence of Mexico City

The subsidence of Mexico City was reported in the late 19th century by Téllez Pizarro in 1899, Roberto Gayol in 1925 and José A. Cuevas during the 1920s and 1930s (Hiriart & Marsal, 1969; Zeevaert, 1983; Figueroa, 1990) (Figures 1 and 2). Nabor Carrillo commissioned by José A. Cuevas, conducted a study on the subsidence using the emerging techniques of soil mechanics. He identified the cause as the consolidation of clays due to increased effective stresses caused by water extraction for the city's supply (Jaime, 1988).

In addition to the subsidence of the city, the extraction of groundwater leads to the formation of cracks and vertical fissures in the clay strata that make up the most superficial part of the soil profile in the Valley of Mexico. These clay strata shrink differentially. Evidence of these cracks is found on the surface in Lake Texcoco, Ecatepec, Colonia Roma, Coapa, Tláhuac, Xochimilco, Iztapalapa, and other areas. Systematically, these cracks are also observed in undisturbed subsurface samples and may be related to the loss of drilling mud in geotechnical borehole logs. Cracks frequently appear at the boundaries of the ancient lake with the surrounding mountains and volcanoes in the Valley of Mexico. These effects have been studied by various authors such as Juárez-Badillo (1961), Marsal & Mazari (1959), Figueroa (1976), Zeevaert (1983), Cabral-Cano *et al.* (2008), Auvinet *et al.* (2014), Chaussard *et al.* (2014), Chaussard *et al.* (2021), and Solano-Rojas *et al.* (2015).

Based on the above, it can be inferred that the properties of the clays in the Mexico basin are in a state of continuous evolution—from the deeper strata to the surface—with respect to water content, shear strength, compressibility, and dynamic characteristics, as noted by Jaime (1988), Ovando-Shelley *et al.* (2007), Aguilar (2008), and Mayoral *et al.* (2019). Furthermore, Ovando Shelley *et al.* (2013), Carréon-Freyre *et al.* (2020) discussed the damage caused by differential settlements due to subsidence and changes in soil properties to historical monuments in Mexico City, which is exacerbated during earthquakes.

The most significant impact of the city's subsidence occurs on the foundations. In partially or fully compensated foundations, the reduction in pore pressure combined with the stresses induced by the foundation causes the preconsolidation pressure of the clay to be exceeded. Consequently, the clay starts to behave along the virgin compression curve, resulting in an increase in vertical deformations.

The most systematic investigations to identify and evaluate subsidence were initiated by Carrillo, 1947, using piezometers and benchmark leveling. Subsequently, Marsal *et al.* (1952), and Marsal & Mazari (1959), continued these studies. Various authors such as Reséndiz *et al.*, (1970), Figueroa (1976, 1990),

Nader & Morales (1978), Murillo & García (1978), Ortega-Guerrero *et al.* (1999), Ovando-Shelley *et al.* (2003), Santoyo *et al.* (2005), and Auvinet *et al.* (2017), have studied the regional subsidence of Mexico City and the Valley of Mexico, as well as its effects on buildings and municipal services. Additionally, the Mexican Society of Geotechnical Engineering has held specialized meetings and symposia on this topic in the years (SMMS, 1970, 1978, 1990, 1991).

Numerous studies have analyzed land subsidence in Mexico City using InSAR and DInSAR methodologies, as it is one of the most studied regions worldwide for ground deformation. More recently Cabral-Cano *et al.* (2008), Chaussard *et al.* (2014, 2021), Solano-Rojas *et al.* (2015), and Cigna *et al.* (2020), among many others.

Different studies have shown that earthquakes cause sudden settlements and accelerate and promote the appearance of surface cracks. Marsal and Mazari (1959) identified these settlements caused by the July 1957 earthquake in various constructions. Subsequently, Zeevaert (1983) and Jaime *et al.* (1987) documented the occurrence of sudden soil settlements following an earthquake. Recently using DInSAR technology Solano-Rojas *et al.* (2020).

Zeevaert (1983) describes the case of a building with a partially compensated foundation, which experienced sudden settlement after the 1957 earthquake and an increase in its subsidence rate (Figure 3). Zeevaert indicated that the static shear stresses combined with the dynamic shear stresses induced during the July 1957 earthquake reached the ultimate shear strength of the silty clay deposit. As a result, partial damage occurred in the soil structure, leading to an increase in the compressibility of the material, which caused the observed consolidation phenomenon.

Jaime *et al.* (1987) studied the settlements of a four-story heavy building in the Roma neighborhood of Mexico City. The structure was built in 1982 and experienced settlements of 0.18-0.24 m over a period of 32 months, causing damage to an adjacent lightweight structure. As a result, periodic topographic surveys were conducted, and several benchmark leveling points were installed around the building and the block where it was located, as shown in Figure 4. The building site was situated facing a small park (free of structures), so the reference benchmark was located centrally within it. Although the reference benchmark was not strictly a fixed point due to the regional subsidence of Mexico City affecting it, this effect also manifested in the building and the entire block under study, thereby canceling out its impact.

The settlement over time of typical points is shown in Figure 5. From May to September 1985, the settlement rate of the structure was 0.045 m/year, while that of the block was zero. After the September earthquakes, the settlement-time curves exhibit a sudden vertical movement of the structure averaging 0.022 m.

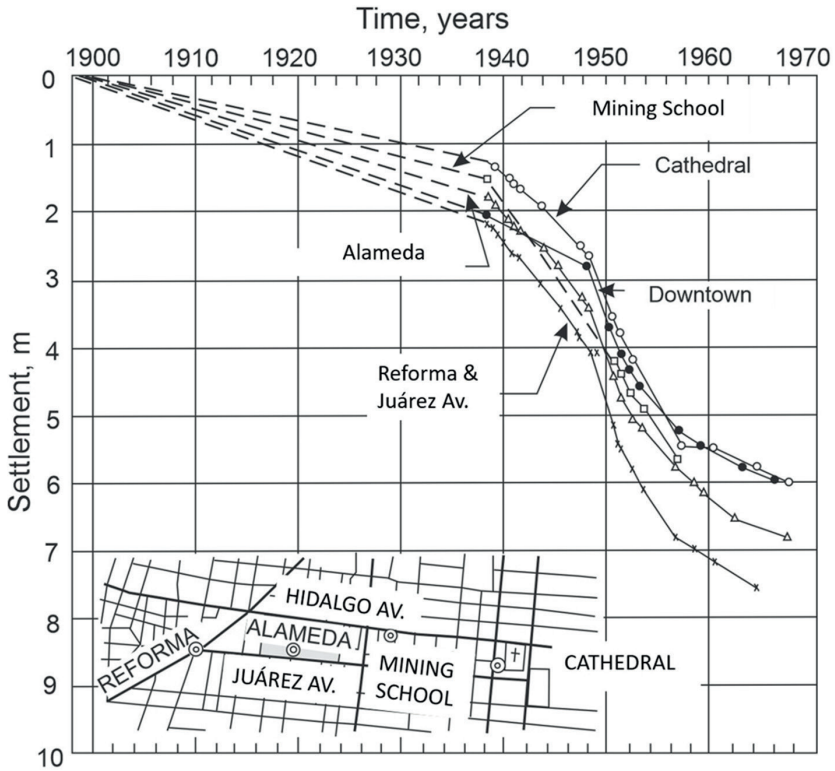


Figure 1. Benchmarks settlements during the period of 1898-1966 (Hiriart & Marsal, 1969).

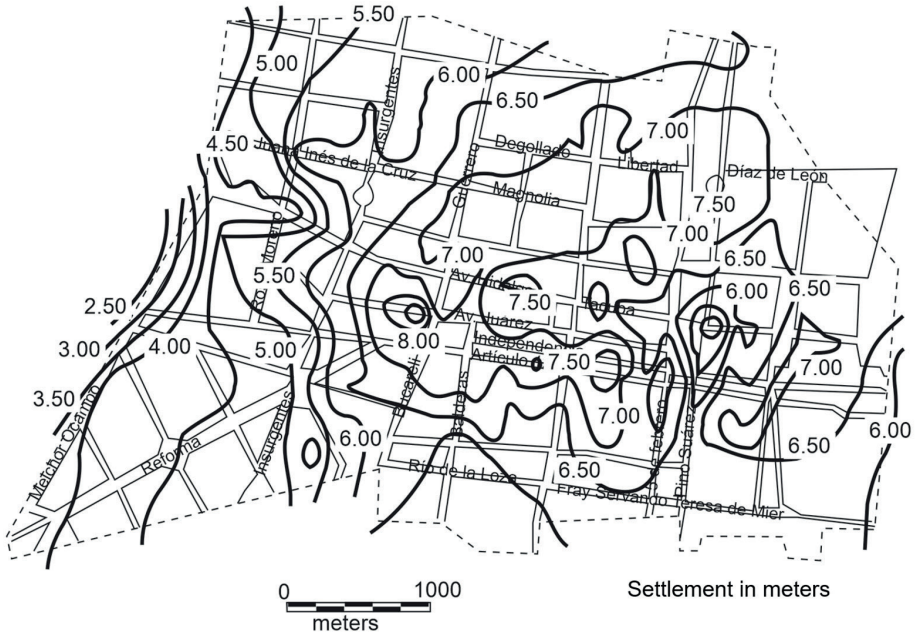


Figure 2. Settlements in Mexico City during the period of 1891-1966 (Hiriart & Marsal, 1969).

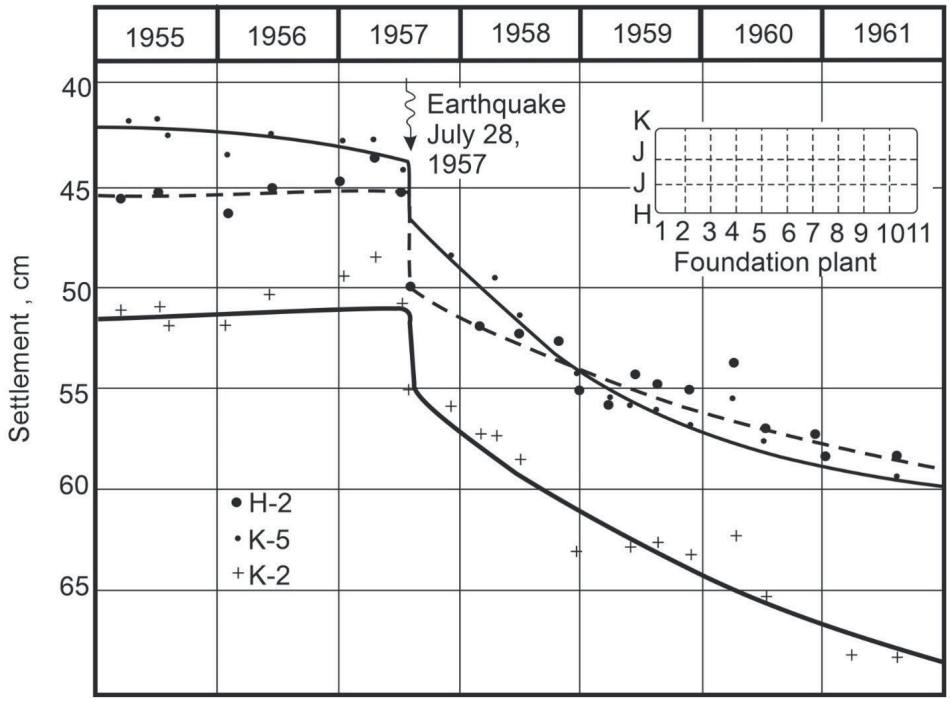


Figure 3. 1957 Mexico City Earthquake, effect on the settlement of a building (Zeevaert, 1983).

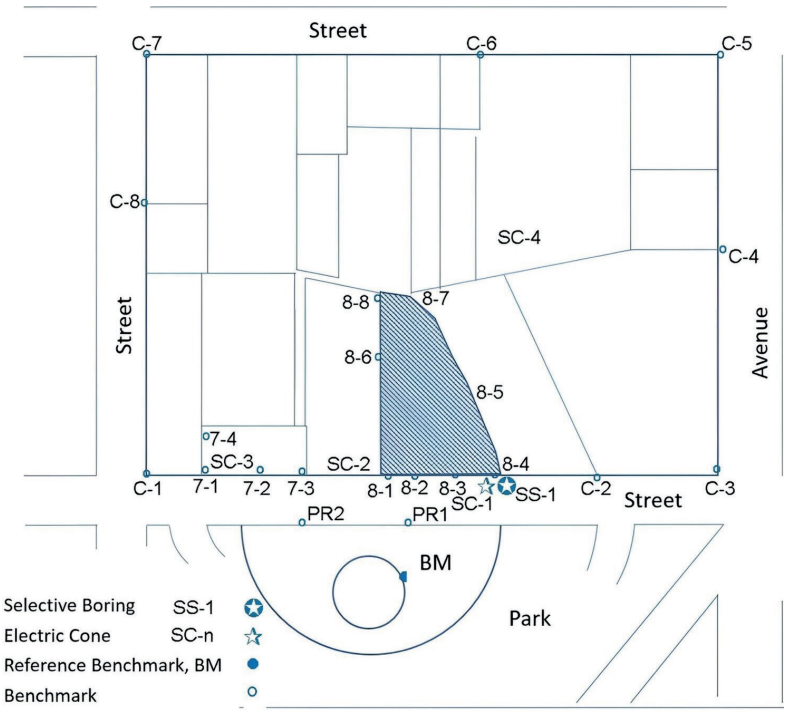


Figure 4. Location of the studied building and of the benchmarks (Jaime *et al.*, 1987).

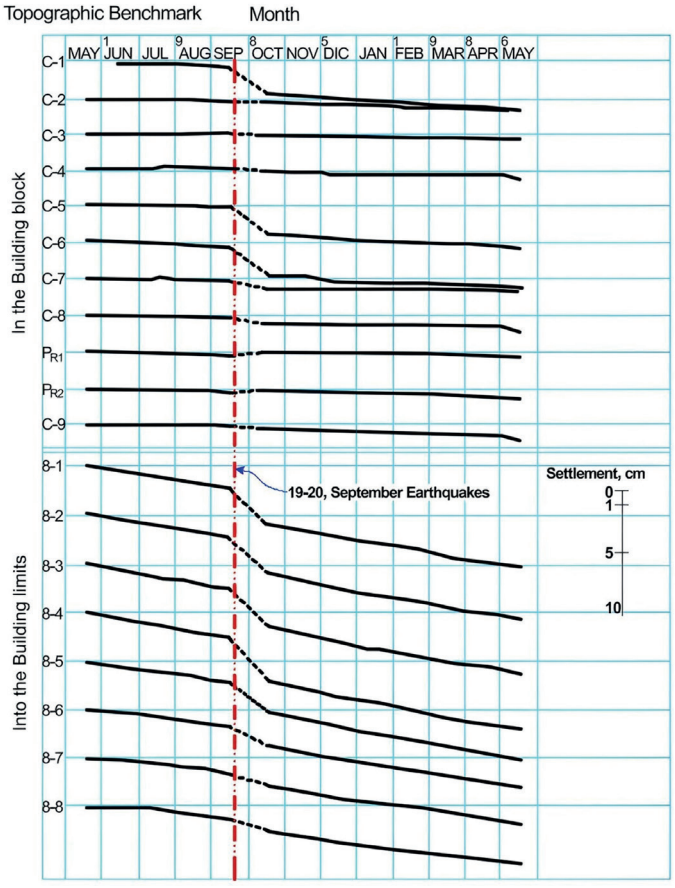


Figure 5. Results of leveling at different benchmark points (Jaime *et al.*, 1987).

The subsequent leveling survey in October, when access to the site was possible, showed that the entire block settled between 0.01 and 0.028 m relative to the reference point. In the months following until 1986, the vertical movement rate of motion of the structure returned to its pre-earthquake rate, while relative movement in the block ceased.

According to the description, earthquakes induce immediate settlements both in open areas and within the influence zone of buildings and structures. As observed in various zones of Mexico City, they also trigger the sudden appearance of cracks that had not previously manifested and exacerbate the deformation of existing cracks.

3. Satellite Image Processing

In this research, SAR satellite images were used. These satellites are equipped with an active sensor radar. The satellites have fixed orbits between 600 and 800 km above the Earth's surface and travel their orbit at fixed times; therefore, they pass over the same location at the same period.

3.1 Methodology

The satellite images were processed using the freely available SNAP software (Sentinel Application Platform). Developed by the organizations Brockmann Consult, SkyWatch and C-S. The general sequence for determining relative subsidence maps is summarized below (Braun & Vecci, 2021; Serco, (2018):

1) Obtaining the Differential Interferogram (Figure 6a)
    a. Preparation of the images. The principal and secondary images are read. In both, the bursts belonging to the area of interest are selected and precise orbital information is applied to them (e.g., the location of the satellite during the acquisition of the images).
    b. Stacking or co-registering images. Coregistration is the process of aligning SAR images with sub-pixel accuracy to enable the precise estimation of phase differences between the reference and secondary acquisitions. This process utilizes both orbital metadata and a Digital Elevation Model (DEM), which are automatically downloaded by SNAP. Based on this information, the images are spatially aligned and georeferenced according to the selected DEM. The orbital data are incorporated through the "Apply Orbit File" operator, which downloads the precise orbit files automatically. The DEM used is the Shuttle Radar Topography Mission (SRTM) 1Sec HGT (NASA JPL, 2000), valid for latitudes between 60° North and 54° South, which includes the territory of Mexico. Bilinear interpolation was employed as the resampling method.
    c. Extraction of the flat-earth phase. The curvature of the Earth is estimated by the use of metadata and subtracted from the Complex Interferogram.
    d. Extraction of the topographic phase. A digital elevation model (e.g. the SRTM 1sec HGT) is used to subtract the topographic phase and the consistency calculation is performed. The Differential Interferogram is obtained.
2) Processing of the Differential Interferogram to determine displacements in the Line Of Sight (LOS) direction (Figure 6b):
    a. Goldstein filter application (Goldstein & Werner, 1998). It allowed to minimize the atmospheric and noise contributions of the Differential Interferogram.
    b. Phase development. With the SNAPHU algorithm (Stanford University, 2019) the whole number of cycles is removed or added to the Differential Interferogram to determine the phase developed.
    c. Phase-to-offset conversion. This process converts the unfolded phase of radians to metric units. As a result, the displacements in the LOS direction are obtained.
    d. Terrain correction. In this process, geometric distortions of SAR images are corrected using a digital elevation model (DEM); in addition, they are geolocated in a georeferenced system (e.g., WGS84).
3) Geometric correction of displacements in the LOS direction to determine subsidence. Offset in each pixel is corrected to determine relative settlement. It is necessary to establish a reference point of zero subsidence and correct the rest with respect to that reference point.

4. Estimation of Regional Subsidence by Means of Dinsar

4.1 Satellite information

The satellite images were obtained from the European Space Agency's ASF Data Search Vertex database and were captured by the Sentinel-1A satellite (Serco, (2018) (NASA-ESA, 2021). They were acquired in IW (interferometric wide swath) mode. The footprint is approximately 250 kilometers in an SLC (Single Look Complex) format with a nominal resolution of 5 meters in the direction of the range (perpendicular to the satellite's path) and 20 meters in the direction of the azimuth (in the direction of the satellite's orbit).

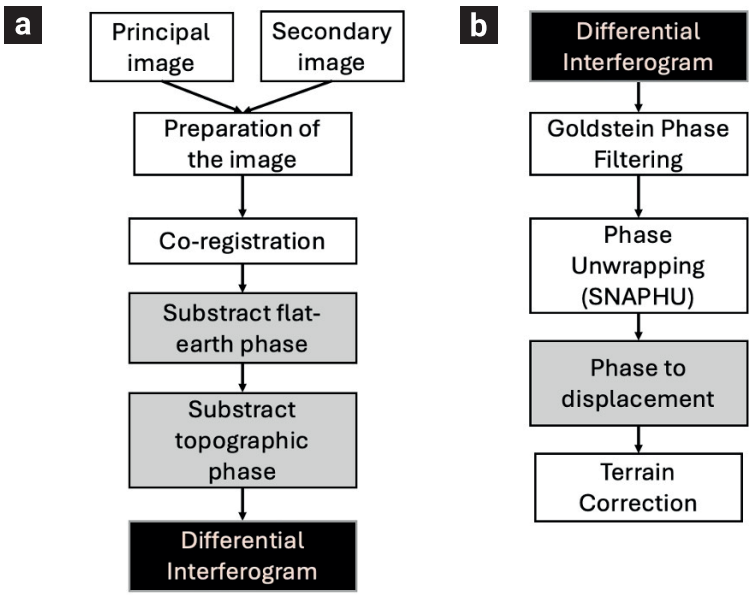


Figure 6. General sequence to determine the Differential Interferogram and the displacements in the LOS direction.

The analyses were done for two periods of time: one for a year and the other for a month. The analysis by year was carried out for the year 2016, the analysis by month was made for the months of August, September, October and November of 2017. This monthly analysis was carried out to determine the subsidence associated with the September 2017 earthquakes. Table 1 summarizes the characteristics of the pairs of images used.

With this information, the following interferograms were obtained to estimate subsidence (Table 2).

To verify the relative annual subsidence obtained by DInSAR, it was compared with leveling done with conventional topography.

Table 1. Information of the images used.

Analysis	No.	Satellite	Date of capture	Address	Track	Orbit
By year	1	S1A	January 26, 2016	Descendant	143	14915
	2	S1A	January 20, 2017	Descendant	143	9665
By month	3	S1A	July 31, 2017	Descendant	143	17715
	2	S1A	August 24, 2017	Descendant	143	18065
	3	S1A	September 5, 2017	Descendant	143	18240
	4	S1A	September 29, 2017	Descendant	143	18590
	5	S1A	October 23, 2017	Descendant	143	18940
	6	S1A	November 4, 2017	Descendant	143	19115
	7	S1A	November 28, 2017	Descendant	143	19465

Table 2. Interferograms obtained.

Análisis	Period	Principal image	Secondary Image
By year	2016	1 (01/26/2016)	2(01/20/2017)
By month	August 2017	1 (07/31/2017)	2 (08/24/2017)
	September 2017	3 (09/05/2017)	4 (09/29/2017)
	October 2017	4 (09/29/2017)	5 (10/23/2017)
	November 2017	6 (11/04/2017)	7 (11/28/2017)

4.2 Analysis of subsidence due to the earthquake of September 19, 2017

Figures 7 and 8 show the relative subsidence determined for August and September 2017, respectively. As references are the Metropolitan Cathedral and the Mexico City Airport (AICM). In these months, settlements between 0.01 and 0.03 m/month were determined in the soft soil area of Mexico City.

Figures 9 and 10 show the subsidence calculated for October and November 2017, respectively. Settlements between 0.02 and just over 0.04 m/ month were determined.

The analysis was concentrated in the Historic Center of Mexico City where two subsidence profiles were located: a West-East profile, approximately 5 km long that passes through the Alameda Central and the Metropolitan Cathedral, and a North-South profile, approximately 3.6 km long that also passes through the Metropolitan Cathedral. The trace of these profiles is shown in Figure 11.

Figures 12 and 13 show the determined subsidence profiles. In the West-East profile, monthly subsidence of up to 0.011 m greater is observed in September, compared to August, October and November. The difference can be associated with the earthquakes of September 2017. On the eastern side, greater settlements were determined, which coincides with the increase in the thickness of the layer of compressible clay soils in that area. In the Alameda Central, Figure 12, there is little coherence of the images.

In the profile of relative subsidence North-South, Figure 13, settlements up to 0.011 m greater were determined in September with respect to August and the other months, which are also associated with the earthquakes of September 2017.

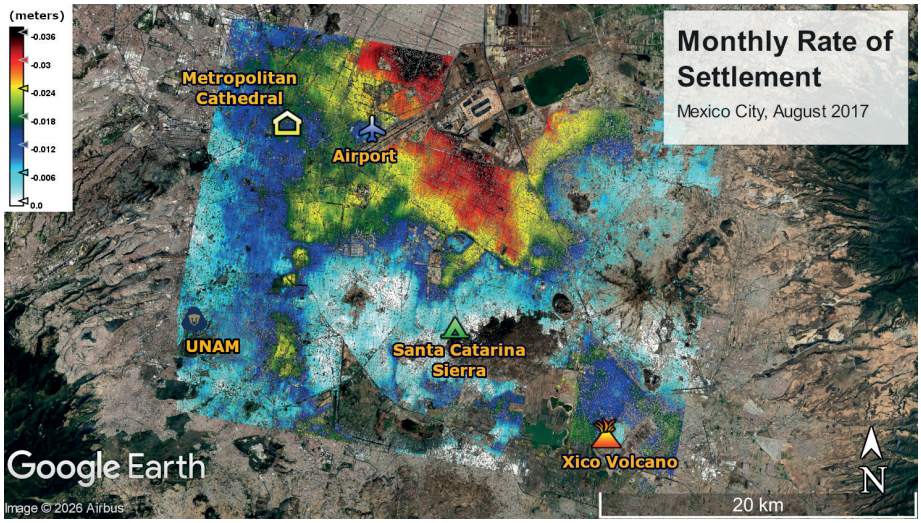


Figure 7. Relative subsidence (m/month) in Mexico City, August 2017.

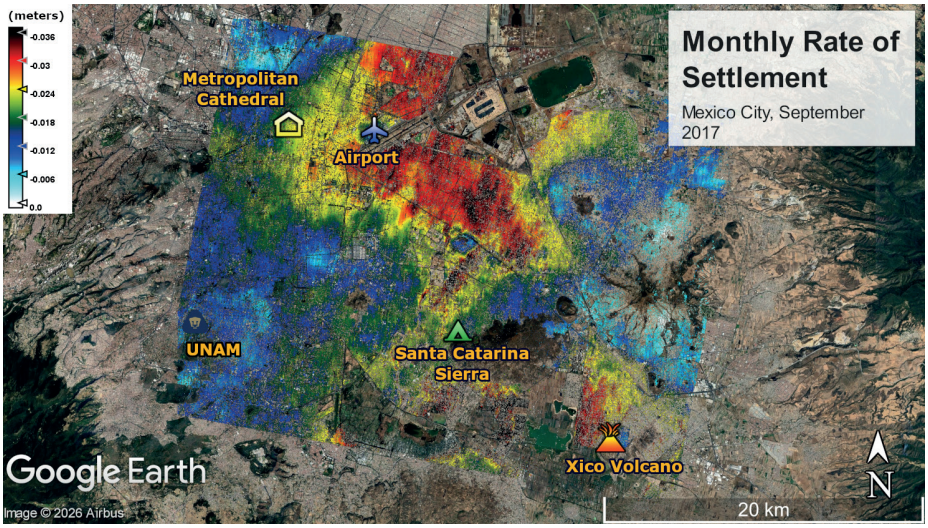


Figure 8. Relative subsidence (m/month) in Mexico City, September 2017.

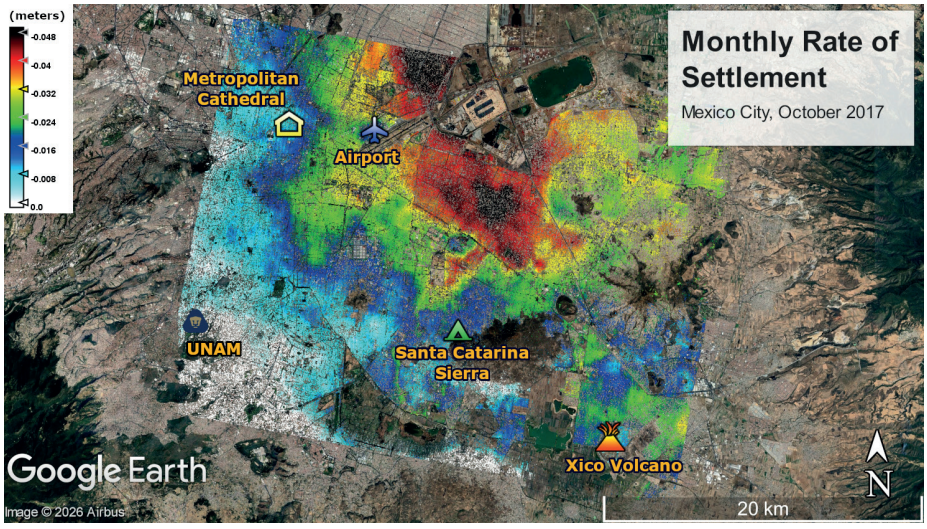


Figure 9. Relative subsidence (m/month) in Mexico City, October 2017.

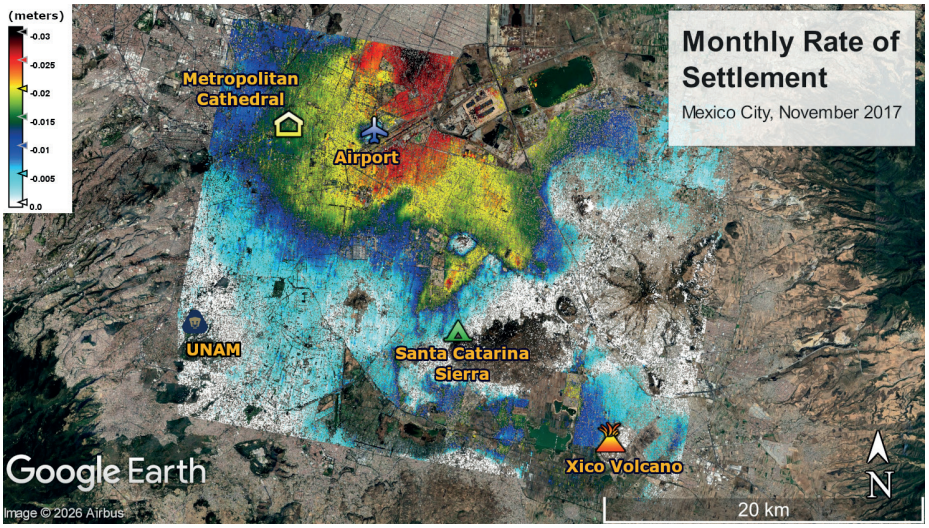


Figure 10. Relative subsidence (m/month) in Mexico City, November 2017.



Figure 11. Plan view of the settlement profiles: West-East and North-South.

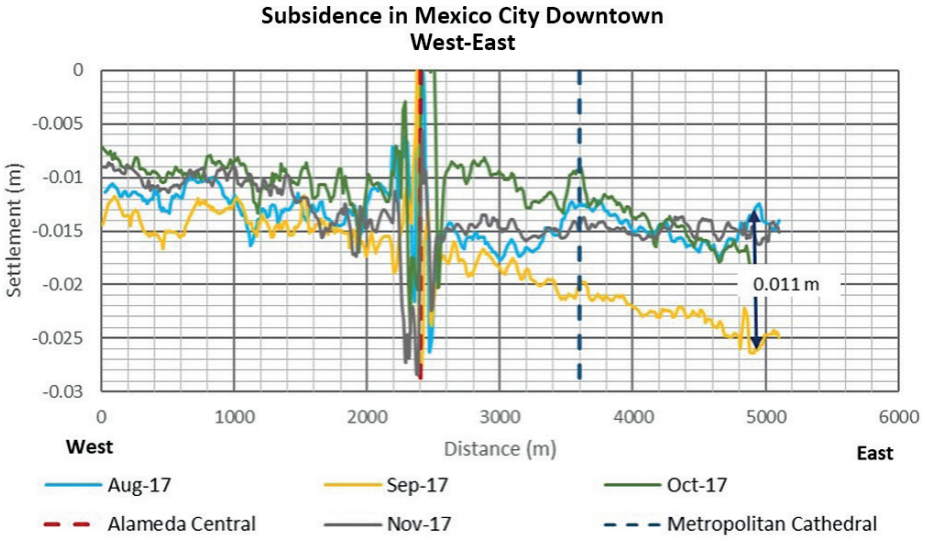


Figure 12. Relative subsidence (m/month) in the Historic Center of Mexico City. West-East profile.

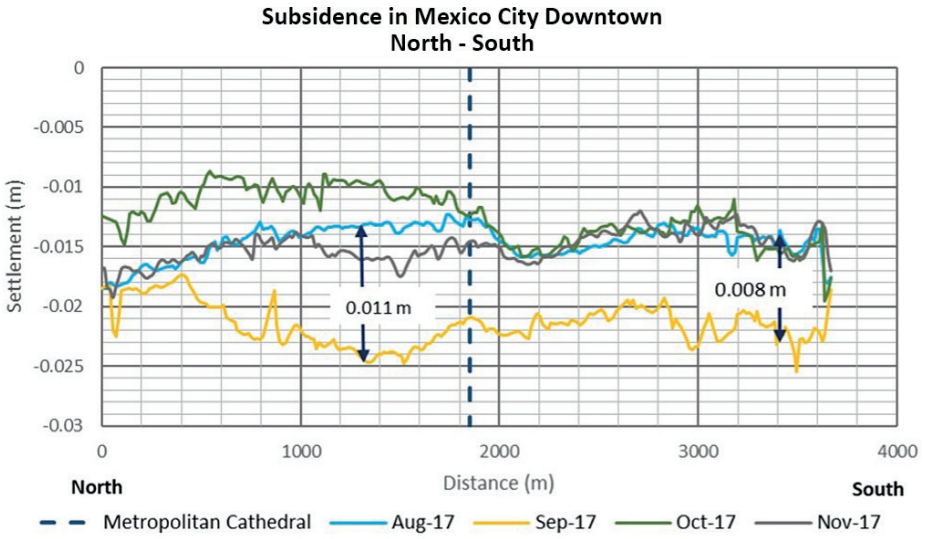


Figure 13. Relative subsidence (m/month) in the Historic Center of Mexico City. North-South profile..

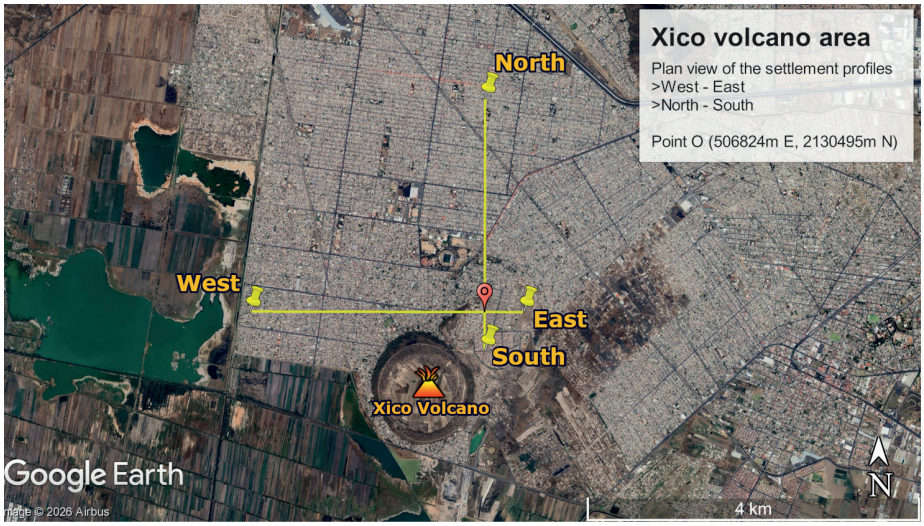


Figure 14. Trace of the subsidence profiles in the Volcano Zone. West-East and North-South profiles.

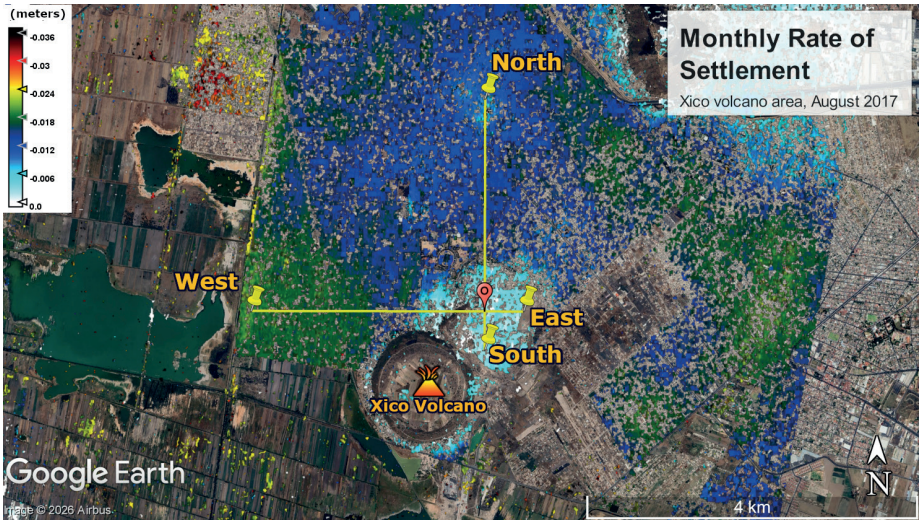


Figure 15. Relative subsidence (m/month) in the Xico Volcano Area, August 2017.

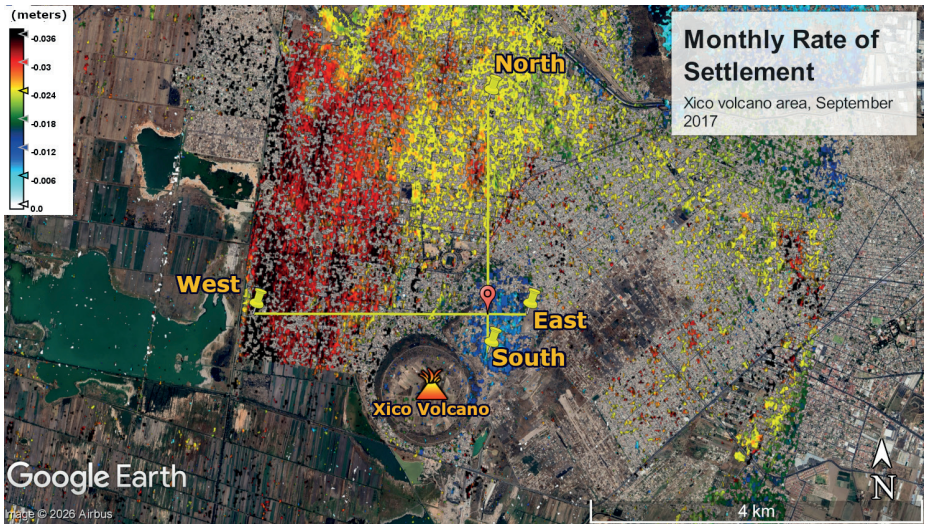


Figure 16. Relative subsidence (m/month) in the Xico Volcano Zone, September. 2017.

4.3 Analysis of subsidence due to the earthquake around the Xico volcano

Similarly, an analysis of settlements in two profiles was also carried out: West-East and North-South in the area around the Xico volcano. Figure 14 shows the traces of these profiles, whose lengths are approximately 3 km. Likewise, a point O (506824 m E, 2130495 m N) is marked as a reference at the intersection of these profiles.

Figures 15, 16, 17 and 18 show the monthly subsidence maps determined for the months of August, September, October and November 2017, respectively. It is observed that, for the months of August, October and November, the determined subsidence varies between 0.005 and 0.02 m; while, for the month of September they reach 0.035 m.

Figures 19 and 20 show the subsidence profiles. The West-East profile shows monthly settlements up to 0.034 m/month higher in September, compared to those obtained in August, October and November. The difference can be associated with the September earthquakes. In Figure 19, 1.1 km from point O to the west, the images have little coherence.

In the profile of relative North-South subsidence, Figure 20, settlements up to 0.017 m/month higher were obtained in September compared to August and the other months, which is also associated with the earthquakes of September 2017.

4.4 Regional subsidence

To estimate the average annual subsidence of SACMEX (2012)-topographic benchmarks, the 2016 bank elevations were

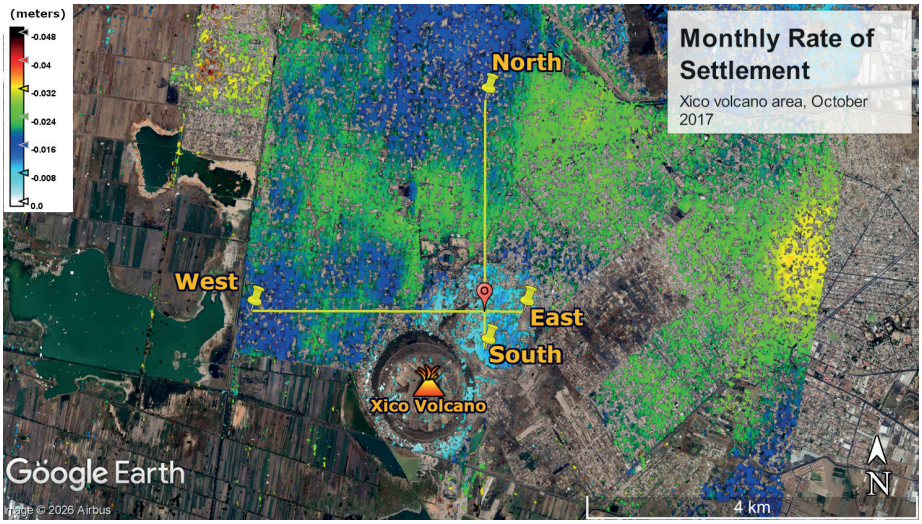


Figure 17. Relative subsidence (m/month) in the Xico Volcano Area, October 2017.

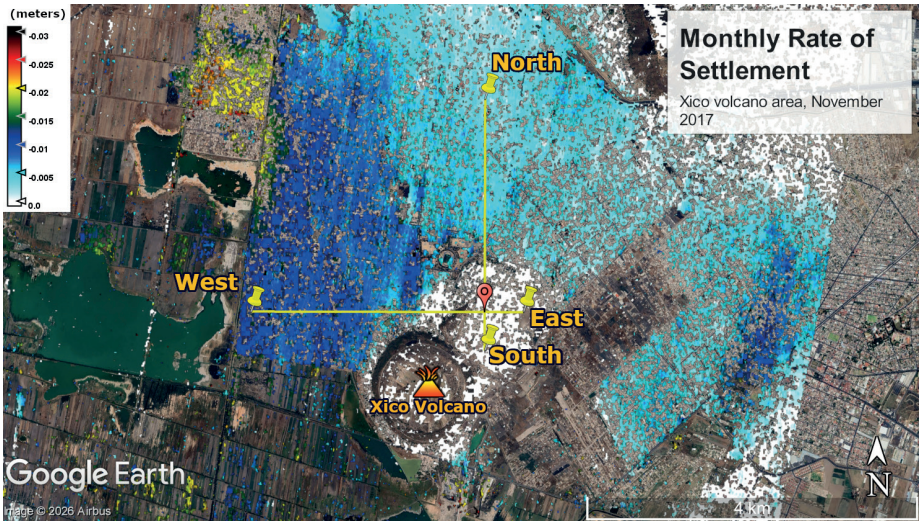


Figure 18. Relative subsidence (m/month) in the Xico Volcano Area, November. 2017.

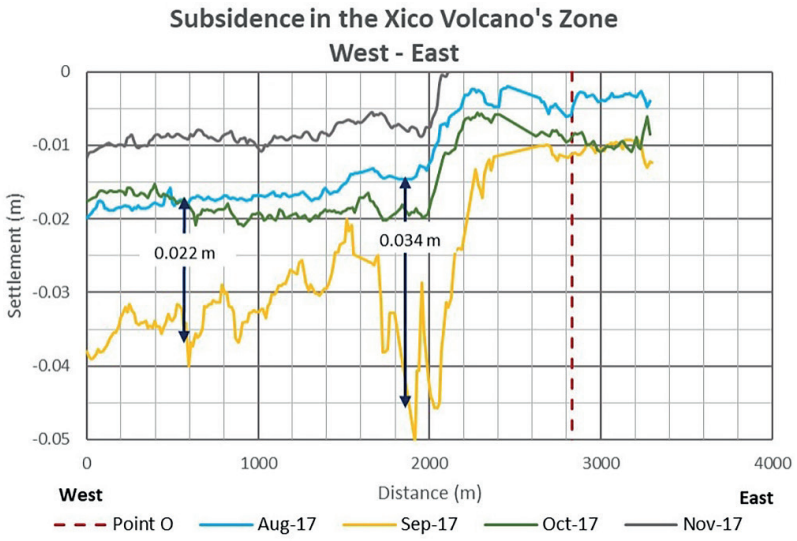


Figure 19. Relative subsidence (m/month) in the Xico Volcano Zone. West-East profiles.

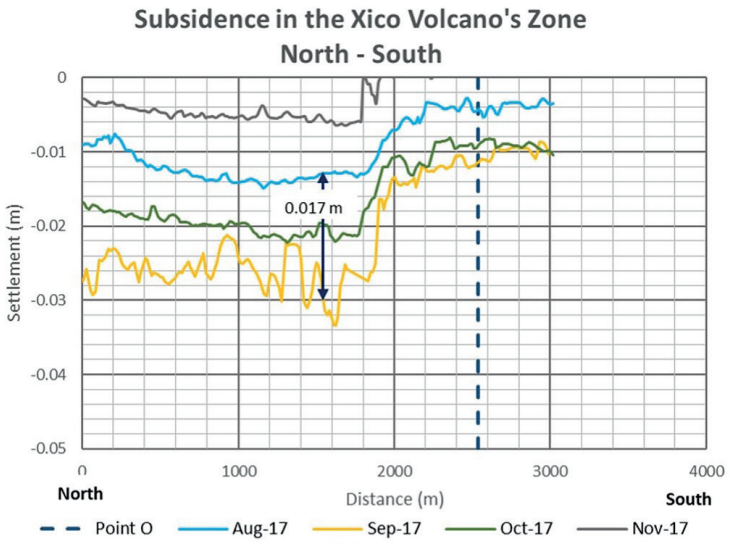


Figure 20. Relative subsidence (m/month) in the Xico Volcano Zone. North-South profiles.

subtracted from those corresponding to 2007 and divided by 9 years. This average annual subsidence was compared with that obtained with the DInSAR analysis corresponding to 2016.

As in the previous section, two annual subsidence profiles were made: one West-East, approximately 5 km long; and another, North-South, of approximately 3.6 km. Both profiles intersect in the Metropolitan Cathedral, as was done in the case of the earthquake subsidence already described. The traces of these profiles are shown in Figures 21, 22 and 24.

Figures 23 and 25 show the subsidence profiles. Minimum subsidence of the order of 0.01 m/year and maximum subsidence of the order of 0.12 m/year were determined in the western and eastern parts, respectively. A trend of subsidence like the average results of the benchmarks is observed. In the West zone there is a good fit in the first 1600 m of the profile, the difference is less than 0.005 m/year. Where there is more dispersion, the difference is about 0.02 m/year.

In the profile of relative subsidence North-South there is little data on benchmarks. The minimum and maximum differences between the average subsidence of benchmarks and the profile obtained by DInSAR for 2016 are approximately 0.005 and 0.02 m/year, respectively.

Table 3 summarizes the data and the average annual subsidence of SACMEX (2012) level banks along the West-East profile.

It should be considered that there may be fluctuation of relative settlements due to changes between rainy and dry periods. When the water table rises, there is a decrease in the effective

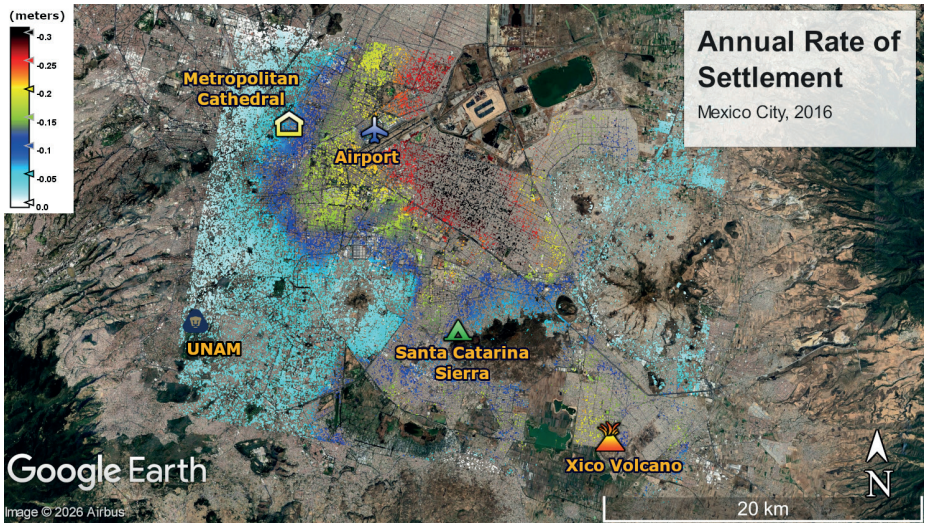


Figure 21. Relative subsidence (m/year) corresponding to the year 2016.



Figure 22. SACMEX benchmarks. West-East Profile.

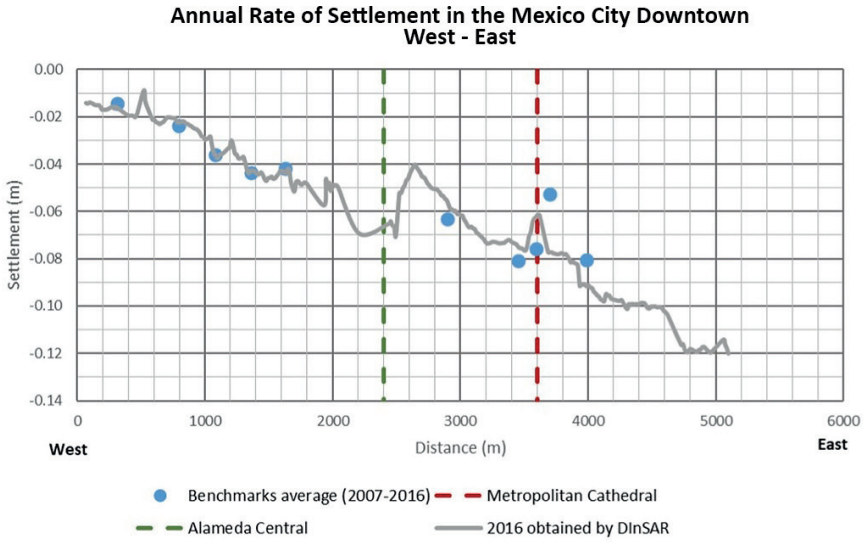


Figure 23. Annual relative subsidence (m/year) in the Historic Center. West-East Profile.



Figure 24. SACMEX benchmarks. North-South Profile

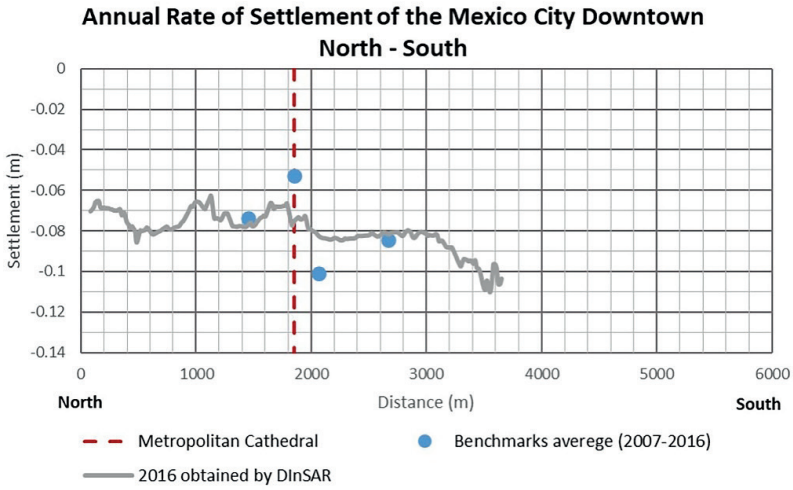


Figure 25. Annual relative subsidence (m/year) in the Historic Center. North-South Profile.

Table 3. Data from the SACMEX benchmarks in the West-East Profile.

BMs	ID	Coordinates UTM (m)		Distance (m)	Elevation 2007 (masl)	Elevation 2016 (masl)	Elevation BM (m)
		East (E)	North (N)				
BN-959	C(N01W02)06	482925	2149807	310	2235.4668	2235.3397	-0.0141
BN-35	B(N01W02)02	483379	2149640	790	2232.7805	2232.5660	-0.0238
BN-956	C(N01W02)02	483646	2149530	1080	2231.3682	2231.0438	-0.0360
BN-960	C(N01W02)10	483882	2149383	1360	2230.1831	2229.7916	-0.0435
BN-32	B(N01W01)05	484200	2149361	1630	2229.0722	2228.6949	-0.0419
BN-953	C(N01W01)16	485400	2149050	2900	2231.2318	2230.6632	-0.0632
BN-935	C(N01E01)02	485914	2148843	3450	2230.2948	2229.5667	-0.0809
BN-939	C(N01E01)06	486055	2148825	3595	2231.8962	2231.2154	-0.0756
BN-946	C(N01E01)13	486152	2148803	3700	2229.6149	2229.1420	-0.0525
BN-04	B(N01E01)04	486451	2148781	3986	2228.2218	2227.4972	-0.0805

stresses of the soil. Likewise, the regime of water extraction from the wells for the supply of drinking water in the city may vary by season. This should be a reason for study considering the data on leveling and the extraction regime per year or month.

Table 4 summarizes the data and the average annual subsidence of (SACMEX, 2012) benchmarks along the North-South profile. The subsidence was determined in a similar way to the corresponding subsidence of the West-East profile.

5. Conclusions

DInSAR technology is an excellent tool for visualizing subsidence in urban areas, particularly in locations that are difficult to access. It allows for more efficient, cost-effective, and timely analysis from a remote setting, compared to conventional field surveying techniques. The comparison between DInSAR results and settlements measured with traditional topography methods show very good concordance.

The earthquakes that hit Mexico City in September 2017 induced sudden settlements in the lake zone of Mexico City. In the Historic Center, these settlements varied between 0.012 and 0.025 m in the free field. In the area of the Xico Volcano, the estimated sudden settlements were between 0.01 and 0.05 m.

From the analyses carried out, in some areas of the city an annual subsidence rate of 0.45 m per year was estimated. Other areas, such as the Historic Center of the City, sink approximately between 0.06 and 0.15 m per year.

Annual subsidence estimates derived from satellite imagery show good agreement with those obtained through conventional topographic surveying.

Subsidence rates vary across the city, with some zones (like Iztapalapa) experiencing up to 0.4 m/year. This variation is due to geological conditions, sediment thickness, and depth to

Table 4. Data from the SACMEX Benchmarks in the North-South Profile.

BMs	ID	Coordinates UTM (m)		Distance (m)	Elevation 2007 (masl)	Elevation 2016 (masl)	Elevation BM (m)
		East (E)	North (N)				
934	C(N01E01)01	485995	2149266	1450	2231.25	2230.59	-0.0736
946	C(N01E01)13	486152	2148803	1855	2229.61	2229.14	-0.0525
947	C(N01E01)14	486129	2148600	2060	2231.30	2230.39	-0.1010
1404	M(S01E01)02	485814	2148068	2665	2228.98	2228.22	-0.0843

the water table.

Differential subsidence causes surface faulting and the formation of fractures that damage urban infrastructure. These faults are often reactivations of pre-existing geological structures and are exacerbated by abrupt changes in subsidence rates.

Ongoing subsidence and related faulting represent a growing hazard to buildings, pipelines, roads, and other infrastructure.

6. References

Aguilar, R. (2008). Dynamic response of the soils of the Valley of Mexico in the future. The new challenges of Geotechnical Engineering in the XXI Century. [Paper presentation]. *XXIV National Meeting of Soil Mechanics*. Mexican Society of Geotechnical Engineering. SMIG.

Auvinet, G., Méndez, E., & Juárez, M. (2017). *The Subsoil of Mexico City-Volumen III*. Institute of Engineering-UNAM.

Auvinet, G., Méndez, E., Juárez, M., Hernández, F., & Martínez, O. (2014). Advances on soil cracking associated with regional subsidence in the Valley of Mexico. [Paper presentation]. *XXVII National Meeting of Soil Mechanics and Geotechnical Engineering*. Jalisco: Mexican Society of Geotechnical Engineering. SMIG.

Braun, A., & Veci, L. (2021). *Sentinel-1 Toolbox-TOPS Interferometry Tutorial*. Skywatch. **https://step.esa.int/docs/tutorials/S1TBX%20TOPSAR%20Interferometry%20with%20Sentinel-1%20Tutorial_v2.pdf**

Cabral-Cano, E., Dixon, T., Miralles-Wilhelm, F., Díaz-Molina, O., Sanchez-Zamora, O., & Carande, R. (2008). Space geodetic imaging of rapid ground subsidence in Mexico City. *Geological Society of America Bulletin*, 120(11-12), 1556-1566. doi: **https://doi.org/10.1130/B26001.1**

Carreón-Freyre, D., Gutierrez-Calderon, R., Cerca, M., and Alcantara-Durán, C. (2020). Factors that condition physical vulnerability to ground fracturing in Mexico City. Proceedings of the International Association of Hydrological Sciences, 382, 571–576. doi: **https://doi.org/10.5194/piahs-382-571-2020**

Carrillo, N. (1947). Influence of artesian wells in the subsidence of Mexico City. *Proceedings of the II International Congress of Soil Mechanics*. Holland.

Chaussard, E., Havazli, E., Fattahi, H., Cabral-Cano, E., & Solano-Rojas, D. (2021). Over a Century of Sinking in Mexico City: No Hope for Significant Elevation and Storage Capacity Recovery. *Journal of Geophysical Research: Solid Earth, 126(4)*, 1-18. **https://doi.org/10.1029/2020JB020648**

Chaussard, E., Wdowinski, S., Cabral-Cano, E., & Amelung, F. (2014). Land subsidence in central Mexico detected by ALOS InSAR time-series. *Remote Sensing of Environment, 140*, 94-106. **http://dx.doi.org/10.1016/j.rse.2013.08.038**

Cigna, F., & Tapete, D. (2020). Present-day land subsidence rates, surface faulting hazard and risk in Mexico City with 2014–2020 Sentinel-1 IW InSAR. Remote Sensing of Environment, 253, 112161. doi: **https://doi.org/10.1016/j.rse.2020.112161**

Figueroa, G. (1976). Subsidence of the City of Mexico; a historical review. *Anaheim Symposium of the International Association of Hydrological Sciences*, California.

Figueroa, G. (1990). Cracks due to overexploitation and subsidence during earthquakes. *Symposium on the subsoil of the basin of the Valley of Mexico and its relationship with foundation engineering five years after the earthquake.* Mexican Society of Soil Mechanics.

Goldstein, R. M., & Werner, C. L. (1998). Radar interferogram filtering for geophysical applications. *Geophysical Research Letters*, 25(21), 4035-4038. doi: **https://doi.org/10.1029/1998GL900033**

Hiriart, F., & Marsal, R. (1969). The sinking of Mexico City-Volume Nabor Carrillo. *Ministry of Finance and Public Trust Credit: Nacional Financiera, 1*, 109-147.

Jaime, A. (1988). *Geotechnics and seismicity in the Valley of Mexico-SD29*. Institute of Engineering-UNAM.

Jaime, A., & Méndez, E. (2002). Evolution of the properties of clay in Mexico City. [Paper presentation]. *XXI National Meeting of Soil Mechanics*. Querétaro.

Jaime, A., Romo, M. P., & Jasso, M. (1987). Seismic Induced Settlement in a Building. [Proceeding]. *VIII Pan-American Congress of Soil Mechanics and Foundation Engineering*, Cartagena.

Juárez-Badillo, E. (1961). Mecanismo de las grietas de tensión en el Valle de México. [Tesis doctoral]. Universidad Nacional Autónoma de México, Facultad de Ingeniería

Marsal, R., & Mazari, M. (1959). *The subsoil of Mexico City.* Mexico City: Institute of Engineering-UNAM.

Marsal, R., Hiriart, F., & Sandoval, R. (1952). *Sinking of Mexico City.*

Observations and analytical studies. Mexico City: ICA.

Mayoral, J., Tepalcapa, S., Román-de la Sancha, A., El Mohtar, C., & Rivas, R. (2019). Ground subsidence and its implication on building seismic performance. *Soil Dynamics and Earthquake Engineering, 126*, 105766. doi: **https://doi.org/10.1016/j.soildyn.2019.105766**

Murillo, R., & García, G. (1978). Ex-lake of Texcoco. *Symposium on the subsoil and foundation engineering in the urban area of the Valley of Mexico*. Mexico City.

Nader, F., & Morales, R. (1978). Ex-lakes of Xochimilco and Chalco. Symposium on the subsoil and foundation engineering in the urban area of the Valley of Mexico. Mexico City.

National Aeronautics and Space Administration-European Space Agency. (2021). *ASF Data Search. Obtained of Earth Data*. [Dataset]. **https://search.asf.alaska.edu/#/**

Ortega-Guerrero, A., Rudolph, D., & Cherry, J. (1999). Analysis of long term land subsidence near Mexico City: Field investigations and predictive modeling. *Water Resources, 35*(11), 3327-3341. doi: **https://doi.org/10.1029/1999WR900148**

Ovando, E., Ossa, A., & Romo, M. (2007). The sinking of Mexico City: Its effects on soil properties and seismic response. *Soil Dynamics and Earthquake Engineering,* 27, 333–343. doi: **https://doi.org/10.1016/j.soildyn.2006.08.005**

Ovando, E., Ossa, A., & Santoyo, E. (2013). Effects of regional subsidence and earthquakes on architectural monuments in Mexico City. *Boletín de La Sociedad Geológica Mexicana, 65*(1), 157-167. **https://doi.org/10.18268/BSGM2013v65n1a12**

Ovando, E., Romo, M., Contreras, N., & Giralt, A. (2003). Effects on soil properties of future settlements in downtown Mexico City due to ground water extraction. *Geofísica International*, 42(2), 185-204. **https://doi.org/10.22201/igeof.00167169p.2003.42.2.264**

Quintanar, L., Krishna Singh, S., Espíndola, V. H., Iglesias, A., Bello Segura, D. I., & Arroyo, D. (2024). Mexico City Earthquake of 11 May 2023 (Mw3.2). Geofísica Internacional, 63(2), 749–762. **https://doi.org/10.22201/igeof.2954436xe.2024.63.2.1757**

Reséndiz, D., Springall, G., Rodriguez, J., & Esquivel, R. (1970). Recent Information on Subsurface Characteristics and Foundation Engineering Practice in Mexico City. [Paper presentation]. *V National Meeting of Soil Mechanics*. Mexico City.

Santoyo, E., Ovando, E., Mosser, F., & Plata, E. (2005). *Síntesis Geotécnica de la cuenca del Valle de México.* TGC Geotecnia.

Serco. (2018). *Land Subsidence with Sentinel-1 using SNAP.* (version 1.2). [Manual]. RUS Copernicus. **https://rus-copernicus.eu/portal/the-rus-library/learn-by-yourself/**

Sistema de Aguas de la Ciudad de México. (2012). *El gran reto del agua en la Ciudad de México.* SACMEX

Sociedad Mexicana de Mecánica de Suelos. (1970). Memorias V Reunión Nacional de Mecánica de Suelos. SMMS.

Sociedad Mexicana de Mecánica de Suelos. (1978). *The Subsoil and Foundation Engineering in the Urban Area of the Valley of Mexico*. SMMS.

Sociedad Mexicana de Mecánica de Suelos. (1990). *El subsuelo de la cuenca del valle de México y su relación con la ingeniería de cimentaciones a cinco años del sismo*. Simposio de la Sociedad Mexicana de Mecánica de Suelos.

Sociedad Mexicana de Mecánica de Suelos. (1991). *Cracking of soils*. Mexico City. SMMS.

Solano Rojas, D., Cabral Cano, E., Hernández Espriú, A., Wdowinski, S., DeMets, C., Salazar Tlaczani, L., Falorni, G., & Bohane, A. (2015). La relación de subsidencia del terreno InSAR-GPS y el abatimiento del nivel estático en pozos de la zona Metropolitana de la Ciudad de México. Boletín de La Sociedad Geológica Mexicana, 67(2), 273–283. doi: **https://doi.org/10.18268/BSGM2015v67n2a10**

Solano-Rojas, D., Cabral-Cano, E., Fernández-Torres, E., Havazli, E., Wdowinski, S., & Salazar-Tlaczani, L. (2020). Remotely triggered subsidence acceleration in Mexico City induced by the September 2017 Mw 7.1 Puebla and the Mw 8.2 Tehuantepec September 2017 earthquakes. [*Proceeding*]. *International Symposium on Land Subsidence (TISOLS)*. doi: **https://doi.org/10.5194/piahs-382-683-2020**

University, Stanford. (s.f.). *SNAPHU: Statistical-Cost, Network-Flow Algorithm for Phase Unwrapping*. (Version 2.0.7) [Computer software]. Stanford Universit. **https://web.stanford.edu/group/radar/softwareandlinks/sw/snaphu/**

Zeevaert, L. (1983). *Foundation Engineering for Difficult Subsoil Conditions. (2ª ed.)*. Van Nostrand Reinhold Company.